Research Article

Enhanced photocatalytic activity of silver vanadate nanobelts in concentrated sunlight delivered through optical fiber bundle coupled with solar concentrator

Joy Sankar Roy[1] · Gabriel Dugas[2] · Steeve Morency[2] · Sidney J. L. Ribeiro[1] · Younès Messaddeq[1,2]

Received: 22 September 2019 / Accepted: 6 January 2020 / Published online: 10 January 2020

Abstract
To date, sunlight driven photocatalytic process for wastewater treatment is a great challenge. Herein, the photocatalytic methylene blue (MB) dye degradation activity of silver vanadate nanobelts has been enhanced using concentrated sunlight irradiation. The MB dye degradation factor in normal and concentrated sunlight irradiation is 0.57 and 0.25 respectively after 120 min of light exposure. Therefore, degradation of MB dye in concentrated sunlight occurs more than two times faster than normal sunlight. The silver vanadate nanobelts have been prepared by simple hydrothermal method. The prepared nanobelts are very thin having length ranging between 5 and 10 µm and width is in the 100–300 nm range. The optical band gap of the synthesized silver vanadate nanobelts is 1.96 eV (632.5 nm), which indicates strong absorption of visible light. This work will open new technological aspects for cost-effective sustainable wastewater treatment using solar energy.

Keywords Silver vanadate · Sunlight driven photocatalysis · Concentrated sunlight · Solar concentrator · Optical fiber · Water purification

1 Introduction

Water is an essential constituent for the survival of human beings, although millions of people worldwide are suffering from lack of fresh and clean drinking water. The ground water and surface water have been polluted by rapid speed of industrialization, expansion of population, unplanned urbanization and environmental pollution [1–4]. The discharge of untreated sanitary and toxic industrial wastes, dumping of industrial effluent, and run off from agricultural fields are the main sources of water pollution [5, 6]. The agriculture and pharmaceutical effluents release pesticides and other chemicals that are responsible for some chronic diseases [5–8]. Various industries such as textiles, dyeing and printing discharge large amounts of synthetic organic dyes as effluents. According to the World Health Organization's (WHO) 2017 report, around 844 millions of people worldwide have no scope to utilize fresh and clean water. In developing countries, almost 70% of all the illness are related to water contamination [9, 10]. Therefore, it is the greatest challenges in twenty-first century for the researchers to develop an eco-friendly, cost-effective and fast processing technology to remove the pollutants from wastewater in order to protect the environment and human beings. To address this serious issue, semiconductor photocatalysis has been believed as a low cost, sustainable and environmentally friendly approach by making use of solar energy [11].

The semiconductor photocatalysts have been studied extensively for purification of wastewater. Among the

✉ Joy Sankar Roy, jsr.phys@gmail.com; ✉ Younès Messaddeq, younes.messaddeq@copl.ulaval.ca | [1]Institute of Chemistry, Sao Paulo State University (UNESP), Araraquara, SP 14800-060, Brazil. [2]Center for Optics, Photonics and Lasers (COPL), Laval University, Quebec, QC G1V 0A6, Canada.

semocinductor photocatalysts, titanium dioxide (TiO_2) is widely used owing its outstanding photocatalytic activity, non-toxicity and high photostability [12–14]. But, TiO_2 is only sensitive under UV-light since it has large bandgap energy of 3.2 eV and utilizes only 4% of available solar energy, which highly restricts its potential application as photocatalyst [14–17]. Therefore, numerous efforts have been made to enhance photocatalytic activity of TiO_2 in visible-light, including anion doping, metal doping, and oxygen deficiency creation [18–20]. Although the light absorption of doped TiO_2 was extended to visible light region, these processes often suffered from thermal instability or carrier-recombination [21, 22]. These methods are not appropriate to develop highly efficient visible-light active photocatalysts. Hence, researchers have devoted much attention to fabricate visible-light driven photocatalysts to enhance the use of solar energy in the process of wastewater purification.

Recently, researchers have developed band structure control technique to fabricate non-TiO_2-based visible-light active photocatalysts, such as $BiVO_4$ [11], $AgNbO_3$ [23], Bi_2WO_6 [24] Ag_3VO_4 [25], $AgVO_3$ [25], $CoFe_2O_4$ [26], $Zr_2Ni_2Cu_7$ [27]. Among thses photocatalysts, silver vanadate has drawn immense interest due to their excellent antibacterial, electrochemical and photophysical properties along with photocatalytic activity [25, 28, 29]. The researchers are still trying to enhance photocatalytic activity of silver vanadate nanomaterials using various techniques [30–33]. In this work, we report the synthesis of silver vanadate nanobelts by a simple hydrothermal method without using any template or surfactant and their photocatalytic activity in the degradation of Methylene Blue under normal and concentrated sunlight irradiation. We have used a solar concentrator coupled with optical fiber bundle to deliver concentrated sunlight to the photocatalytic reactor. Most of the researchers use Xenon arc lamp or fluorescent lamp or LED lamp or solar simulator as visible light source to study photocatalytic activity [23–25, 34, 35]. Recently, some of them studied photocatalysis process in direct sunlight irradiation [26, 27, 36]. This is the first time in literature we are using a novel technology to use concentrated sunlight as visible light source to study photocatalytic activity. The utilization of solar concentrator coupled optical fiber bundle as the concentrated sunlight source provides a promising direction for future applications of low cost and fastest sustainable wastewater purification process.

2 Experimental

2.1 Preparation of photocatalysts

Silver vanadate nanobelts were prepared using simple hydrothermal method. In a typical procedure, 2 mmol of NH_4VO_3 and 2 mmol of $AgNO_3$ was dissolved in 40 mL distilled water seperately and then $AgNO_3$ aqueous solution was mixed dropwise into NH_4VO_3 aqueous solution under magnetic stirring. The resulting suspension was transferred into a 100 mL Teflon-lined stainless steel autoclave and kept at 150 °C for 4 h and then cooled to room temperature. The resulting sample was collected and washed with distilled water and ethanol several times and dried overnight at 70 °C.

2.2 Sample characterization

The morphology of the prepared sample was investigated using field emission scanning electron microscope (JEOL, JSM 7500F) and transmission electron microscope (JEOL, JEM 1230). Structural properties were studied using Selected Area Electron Diffraction (SAED) and X-ray diffraction (XRD). The XRD pattern of the powder silver vanadate nanobelts was studied using Bruker D8 Advance X-ray diffractometer. Raman spectroscopy was recorded using Horiba Jobin–Yvon (HR 800) Micro-Raman under 632.8 nm laser irradiation. The Raman spectrum was recorded in the 100–1200 cm^{-1} wavenumber range. The optical absorption characteristic of the sample was investigated using the Varian Cary 5000 UV–Vis–NIR spectrophotometer. Optical power of normal and concentrated sunlight was measured using Gentec-eo UP55N-300F-H12-D0 power meter. An agilent 1200 Liquid Chromatography Mass Spectrometer (LCMS) was used to identify the intermediates of MB dye during degradation.

2.3 Photocatalytic activity evaluation

The photocatalytic activity of silver vanadate nanobelts was investigated by degradation of MB dye under normal and concentrated sunlight irradiation. The concentrated sunlight has been delivered to photocatalytic reactor through optical fiber bundle coupled with solar concentrator. The used solar concentrator is shown in Fig. 1. It consists main four parts: optical reflector, optical fiber bundle, solar tracker and mechanical support. The optical reflector system consists of two mirrors: primary parabolic mirror and secondary flat mirror. Primary mirror captures sunlight and projects concentrated sunlight on secondary mirror. Secondary mirror projects concentrated sunlight on the top of the optical fiber bundle. The optical fiber are made with pure silica to tolerate high temperature at the focal point of the concentrated sunlight and also to pass UV light. The solar tracker is fixed on the arm of the optical system so that it can track the position of the sun and moves according to the movement of the sun. Photocatalytic reactor consists of two small fans to circulate fresh air, a magnetic stirrer to stir photocatalysts suspended MB dye

Fig. 1 Parabolic mirror based solar concentrator coupled with optical fiber bundle

solution, and an optical fiber bundle covered with pure silicate glass to deliver concentrated sunlight from solar concentrator. The photocatalytic reactor is shown by magnification in Fig. 1.

For photocatalytic degradation of MB dye, 20 mg of silver vanadate was dispersed in 50 ml of 20 ppm MB dye solution under ultrasonication for 2 min, and was kept in the dark place for 2 h to achieve adsorption–desorption equilibrium. At regular intervals of time, aliquots of the suspension were collected and analyzed in UV–Vis–NIR spectrophotometer (Varian Cary 5000).

3 Results and discussion

3.1 Morphology and structure

The morphology of the silver vanadate photocatalysts was observed in FESEM and is ahown in Fig. 2 with different magnification. Figure 2 reveals the high yield and homogeneity of nanobelts structure. The SEM images confirm that no other structure except nanobelts are formed. It can be seen in Fig. 2, that length of the nanobelts ranging between 5 and 10 µm and width is in the 100–300 nm range, and the thickness is in order of few nm. The size of the nanobelts can be better understood from TEM images as shown in Fig. 3. The TEM image of a nanobelt is shown in Fig. 3a and 3b. The length and width of the shown nanobelt is 7 µm and 152 nm respectively.

The SAED was studied to conform the crystalline nature of the silver vanadate nanobelts. The SAED pattern is shown in Fig. 3c. The diffused concentric circles and bright spots on SAED image signifies well polycrystalline nature of the silver vanadate nanobelts. Figure 4 displays the XRD pattern of the prepared silver vanadate nanobelts. All the diffraction peaks of the as-synthesized sample conform to pure β-$AgVO_3$ phase (space group: C12m1, 56861-ICSD) [37]. The $(61\bar{2})$ peak is the strongest one, indicationg possible preferential orientation of β-$AgVO_3$ nanobelts. The XRD pattern confirms the non-exsistence of α-$AgVO_3$ phase or silver in the prepared sample.

Figure 5 shows the Raman spectrum of the prepared silver vanadate nanobelts. The Raman band at 956 cm^{-1} is attributed to symmetric stretching of VO_4 units and the strong band at 886 cm^{-1} originates from either bridging V–O–Ag or O–V–O vibrations [37, 38]. The bridging Ag–O–Ag bond is reflected by 808 cm^{-1} Raman band. The Raman bands at 732 cm^{-1} and 519 cm^{-1} are associated with asymmetric and symmetric stretches of V–O–V bond, respectively. The Raman bands at 336 cm^{-1} and 386 cm^{-1}

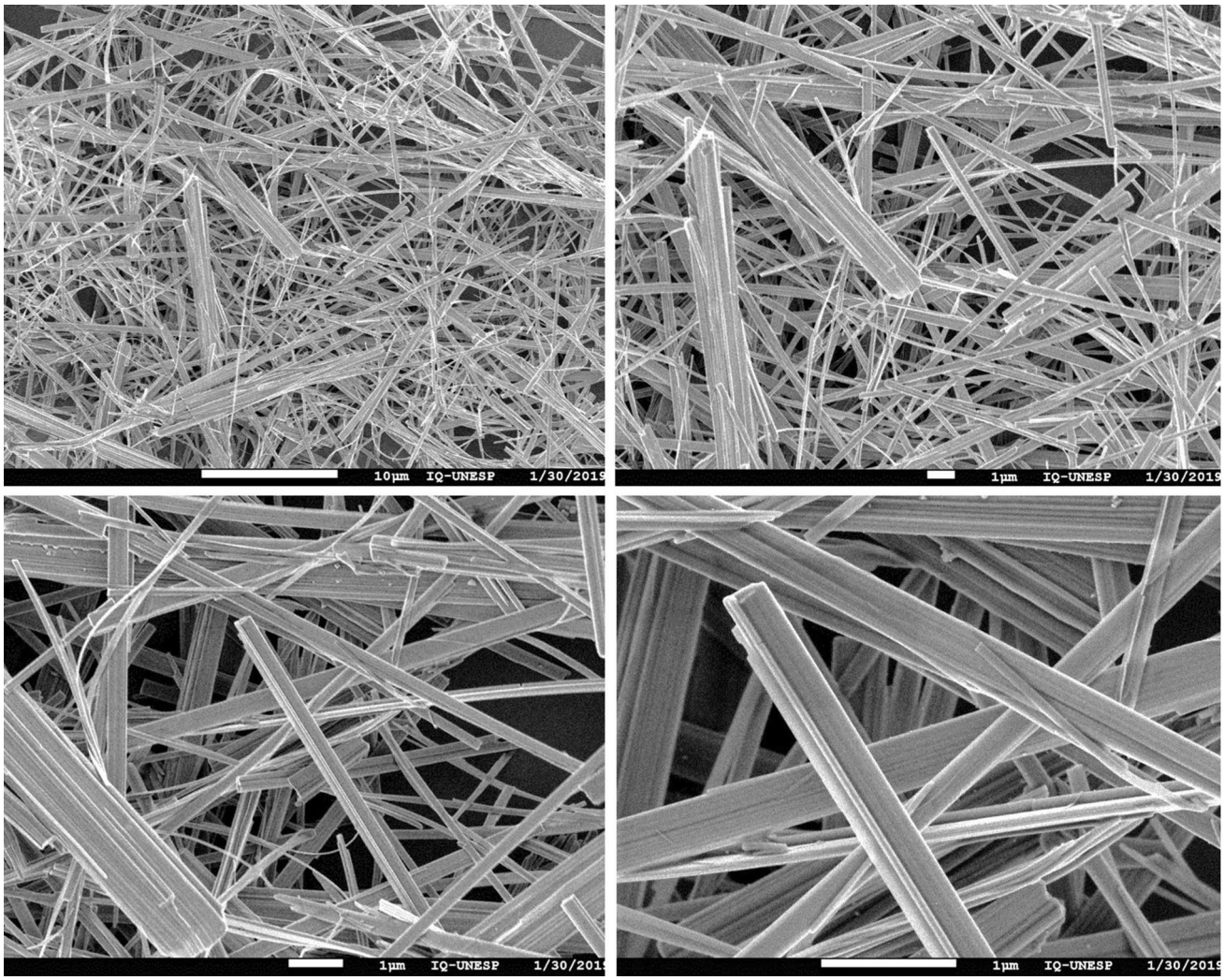

Fig. 2 FESEM images of the β-$AgVO_3$ nanobelts with different magnification

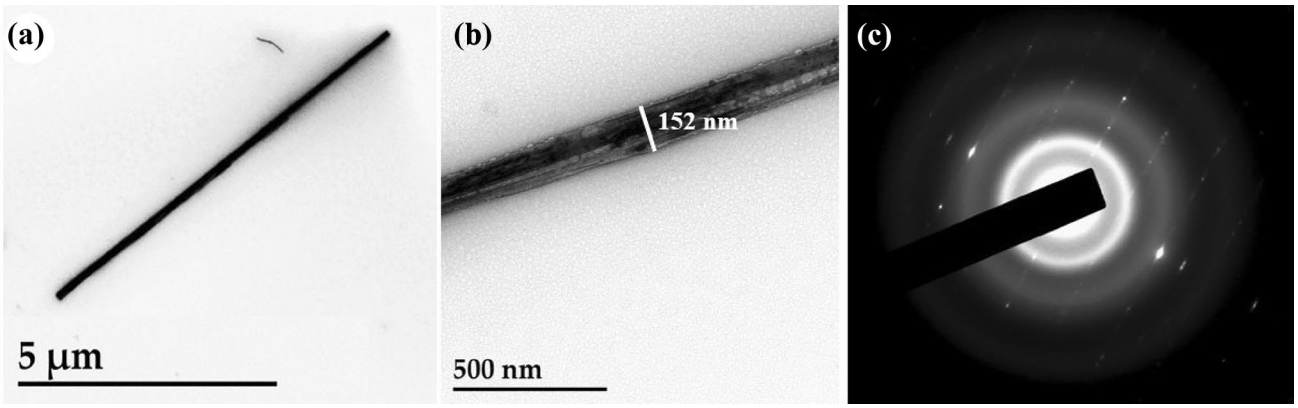

Fig. 3 **a**, **b** TEM images and **c** corresponding SAED pattern of the β-$AgVO_3$ nanobelts

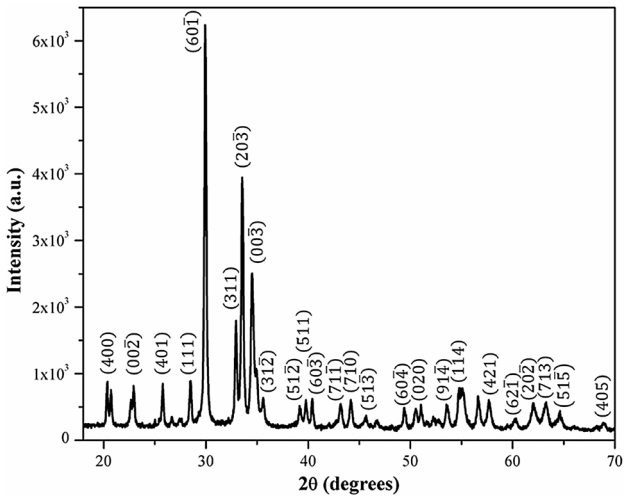

Fig. 4 XRD pattern of the as-prepared silver vanadate nanobelts

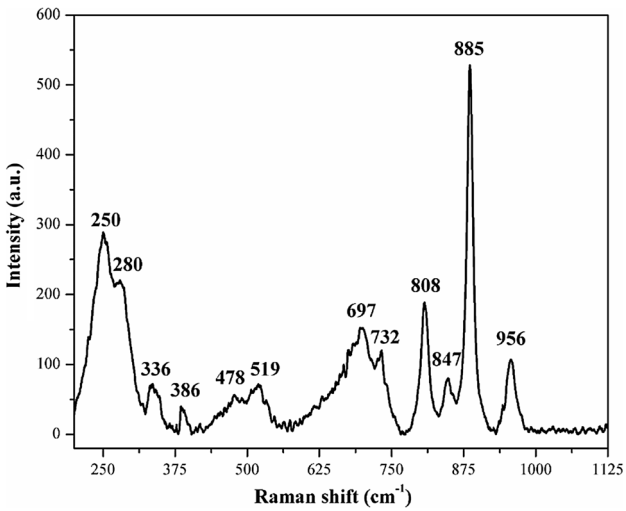

Fig. 5 Raman spectrum of the as-prepared silver vanadate nanobelts

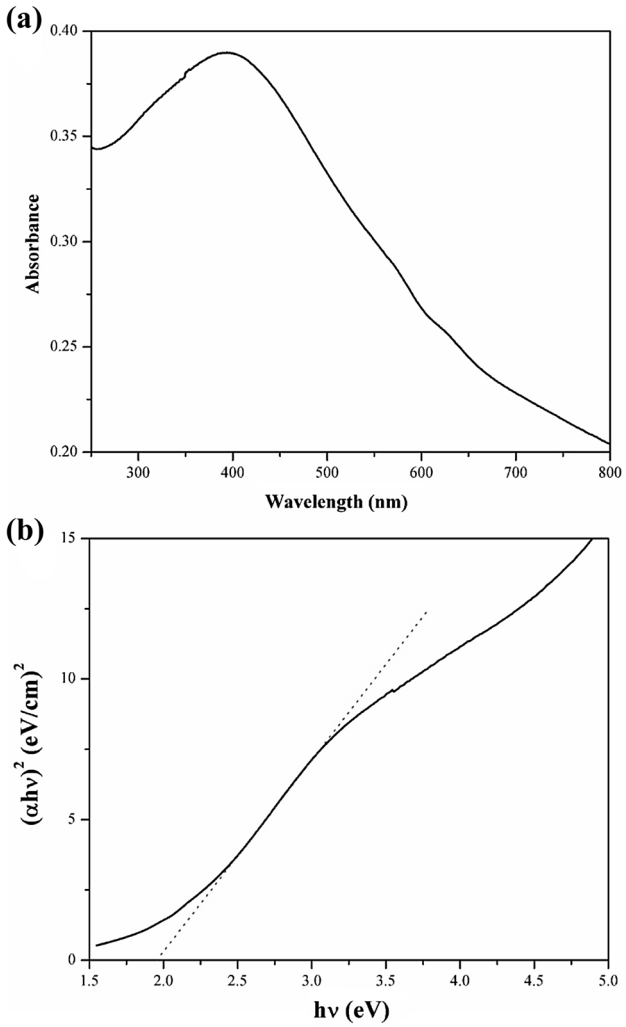

Fig. 6 **a** UV–visible absorption spectrum and **b** Tauc plot of the as-prepared silver vanadate

correspond to the asymmetric and symmetric deformation modes of the VO_4^{3-} tetrahedron, respectively [37]. The symmetric and asymmetric bending modes of the VO_4 units occur at 280 cm^{-1} and 250 cm^{-1}, respectively [38]. The Raman spectrum reflects the pure β-$AgVO_3$ phase of the prepared sample [37, 38].

3.2 Optical properties

The UV–visible absorption spectrum of the prepared silver vanadate nanobelts is shown in Fig. 6a. The absorption

Table 1 Variation of solar irradiance power with wavelength for normal and concentrated sunlight

Wavelength (nm)	Irradiance power (mW/cm^2)	
	Normal sunlight	Concentrated sunlight
632	73.9	324.9
532	72.3	318.6
488	71.5	315.1

band shows maximum at 400 nm, but the absorption edge starts from 650 nm. Therefore, the prepared nanobelts are capable to absorp light in wide range of visible region. To better understand the absorption of optical energy, optical band gap has been calculated using Tauc plot [39–42] as shown in Fig. 6b. The estemated optical band gap is 1.96 eV. Therefore, Fig. 6 reveals that the prepared silver vanadate nanobelts are very much sensitive in visible light.

3.3 Photocatalytic activity

Photocatalytic activity of silver vanadate nanobelts has been studied under direct or natural sunlight and concentrated sunlight irradiation. The irradiance power of used concentrated sunlight is much higher that the normal sunlight. The irradiance power of normal and concentrated sunlight is summarised in Table 1. Though the optical band gap of the silver vanadate nanobelts is 632 nm (1.96 eV), we have measured solar irradiance power for different wavelength like 488 nm, 532 nm and 632 nm because the nanobelts show broad absorption spectrum as shown in Fig. 6. The irradiance power of concentrated sunlight has been measured at distance 18 cm from the optical fiber bundle where the sample was kept for experiment. Photocatalytic activity of the silver vanadate nanobelts for degradation of MB dye under sunlight is shown in Fig. 7. Figure 7a represents comparision of absorbance spectra of MB dye with duration of normal sunlight exposure and similar activity for concentrated sunlight is shown in Fig. 7b. It can be seen from Fig. 7, that the absorbance peak of MB dye decreases gradually with duration of sunlight exposure and it occurs faster for concentrated sunlight. The photocatalytic activity of the silver vanadate nanobelts can be better understood from Fig. 8. Relative degradation of the MB dye is shown in Fig. 8a and time

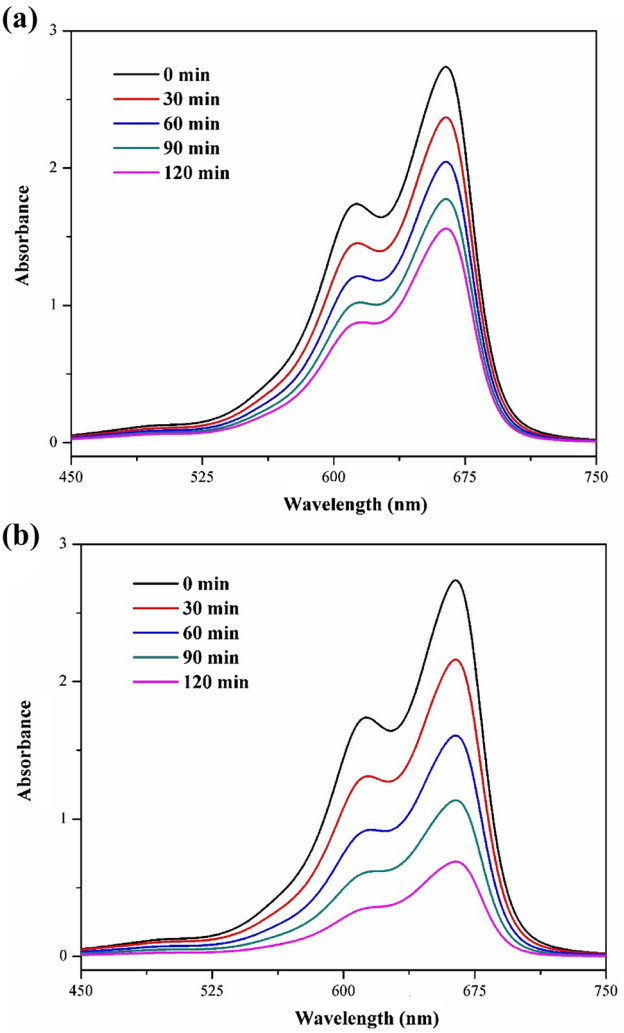

Fig. 7 Comparision of absorption spectra of MB dye after irradiation of **a** normal sunlight and **b** concentrated sunlight

dependent degradation efficiency is shown in Fig. 8b. Relative degradation is expressed by C/C_0, where C is dye concentration after certain duration of light exposure and C_0 is the initial dye concentration. It is clear from Fig. 8 that the degradation occurs faster for concentrated light. The degradation factor for normal and concentrated sunlight is 0.57 and 0.25 respectively after 120 min of light exposure. Therefore, degradation of MB dye in concentrated sunlight is more than two times faster than normal sunlight. The enhancement in MB dye degradation under concentrated sunlight can be clearly understood from

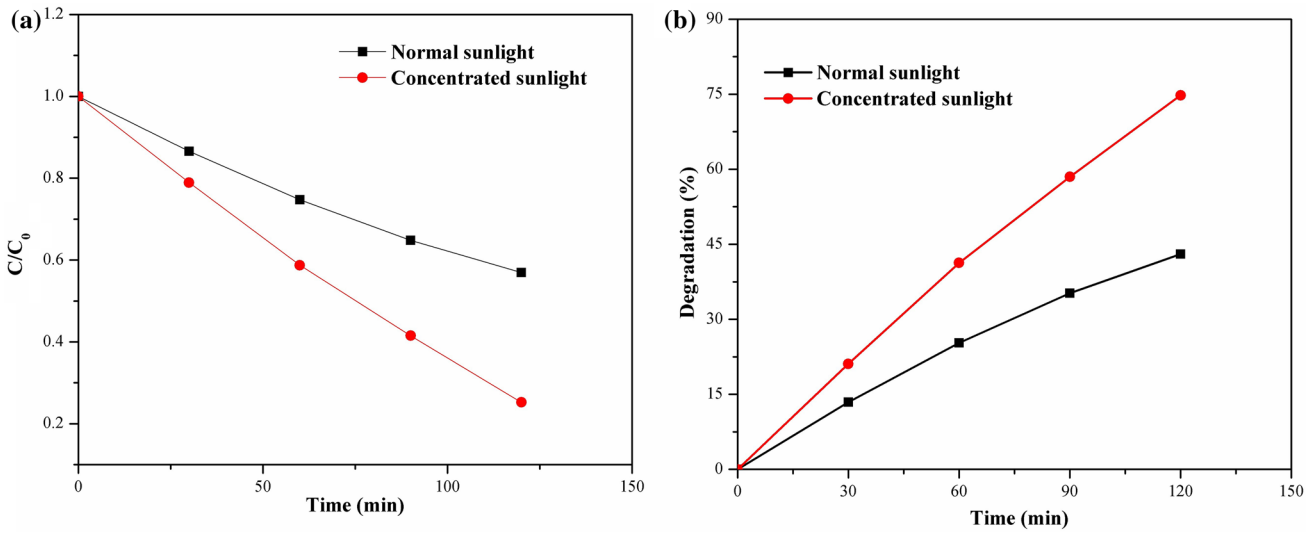

Fig. 8 **a** Relative degradation and **b** corresponding % degradation of MB dye catalized by as-synthesized silver vanadate nanobelts under normal and concentrated sunlight irradiation

Fig. 8b. Silver vanadate nanobelts are capable to degrade 75% of MB dye just within 120 min of concentrated sunlight exposure, where as only 43% degradation occurs for normal sunlight exposure. Recently, Gonzalez-Zavala et al. reported 37% degradation efficiency for Malachite green dye using photocatalytic activity of silver vanadate thin film and they achieved maximum of 53% degradation efficiency by doping silver with silver vanadate thin film after 180 min exposure of light [34]. They used solar simulator to deliver artificial sunlight for photocatalytic activity. Belver et al. reported around 40% degradation of Rhodamine B dye in 420 min using $AgVO_3$ nanoparticles [35]. In our work, we got 75% degradation efficiency for MB dye using concentrated sunlight just within 120 min. Therefore, solar concentrator coupled with optical fiber bundle will open up new technological aspect to utilize solar energy for wastewater treatment.

3.4 Photocatalysis mechanism

The prepared silver vanadate nanobelts absorb sunlight with energy equal to or greater than the band gap energy (1.96 eV) of the silver vanadate and generate electrons and holes in the valence and conduction band respectively. The generated electrons and holes migrate to the surface of the silver vanadate nanobelts and participate in oxidation and reduction process to produce hydroxyl and superoxide radicals respectively. The formed hydroxyl and superoxide radicals react with MB dye to degrade it. The MB dye is degraded to harmless or less-harmful products like carbon dioxide (CO_2), water (H_2O) etc. through some intermediates compounds. These intermediates compunds were identified by LCMS and is shown in Fig. 9. Based on the ratios of mass to charge (m/z) in the mass spectra (Fig. 9), the corresponding compounds and their structural formulas have been deduced and the photocatalytic degradation pathway of MB dye (m/z = 284) has been proposed in Fig. 10.

Based on our experimental results and earlier reports in literature on photocatalytic degradation of organic molecules, photocatalytic degradation mechanism for MB dye using β-$AgVO_3$ photocatalyst is proposed as follows [43, 44]:

$$AgVO_3 + h\nu \rightarrow AgVO_3\left(e^- + h^+\right)$$

$$h^+ + H_2O \rightarrow \cdot OH$$

$$h^+ + OH^- \rightarrow \cdot OH$$

$$e^- + O_2 \rightarrow \cdot O_2^-$$

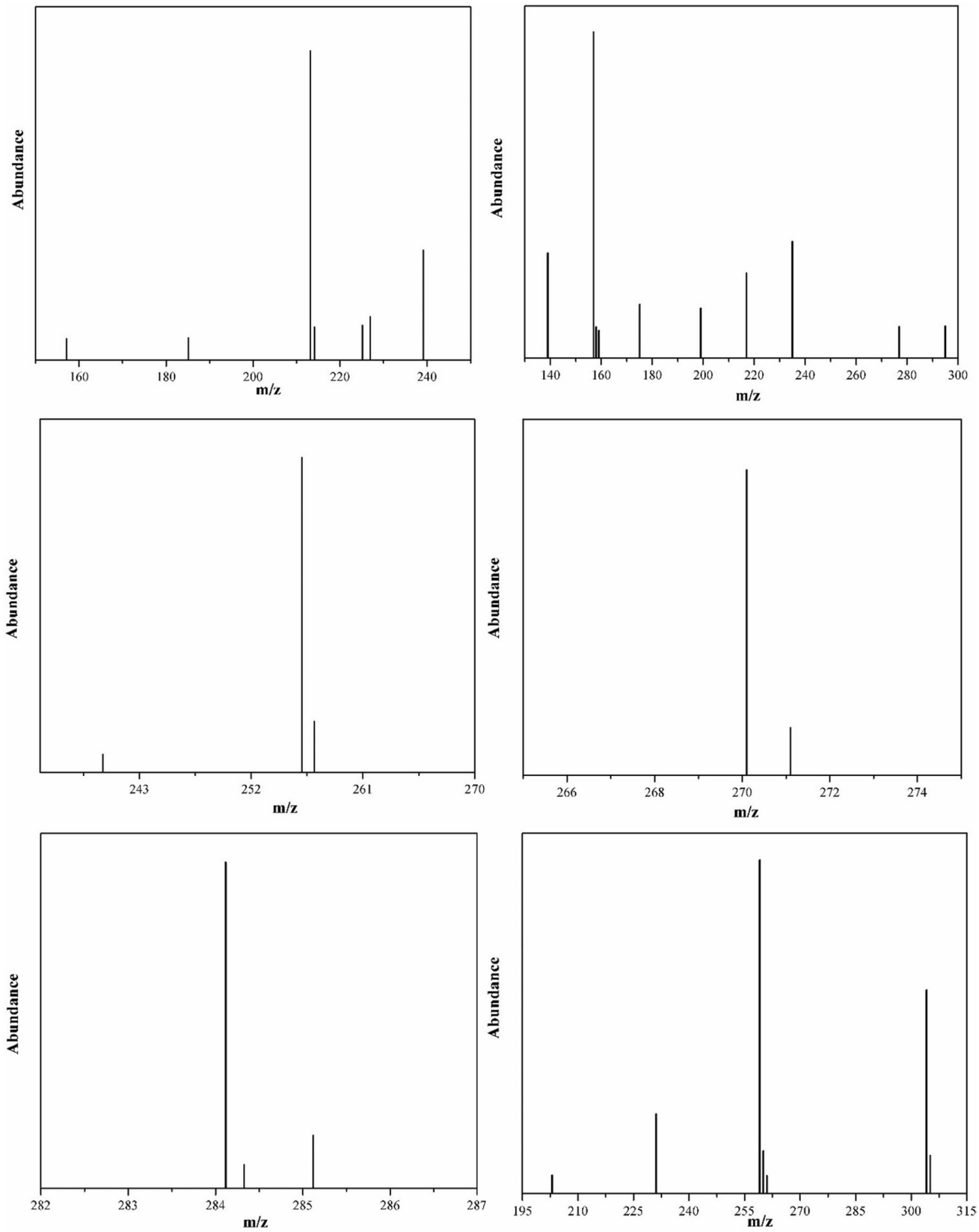

Fig. 9 LC-MS spectra of MB during photocatalytic degradation process

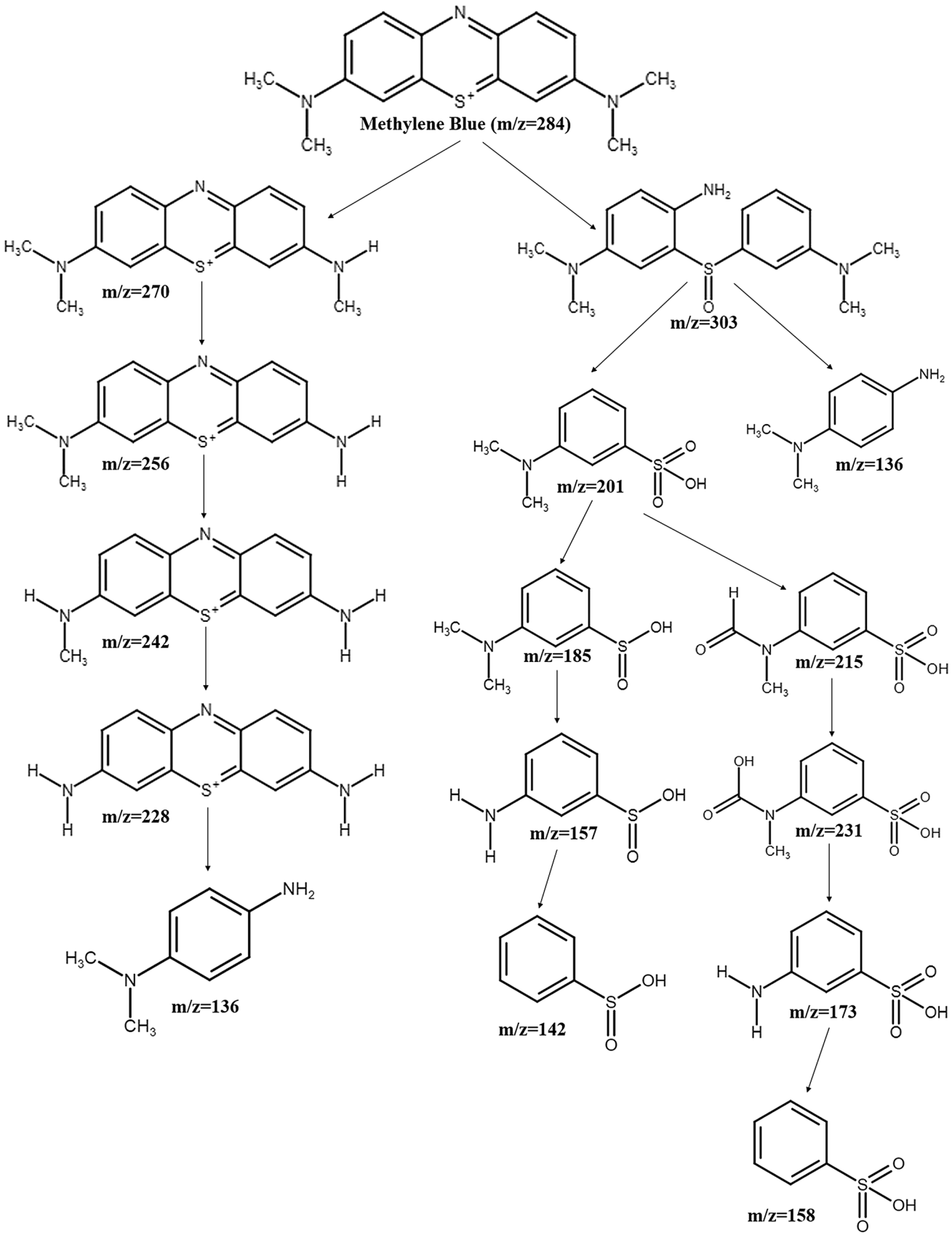

Fig. 10 Possible degradation pathway of MB during photocatalysis

$MB + \cdot OH \rightarrow intermediates \rightarrow degradation\ products$

$MB + \cdot O_2^- \rightarrow intermediates \rightarrow degradation\ products$

Photocatalytic activity of silver vanadate nanobelts enhances in presence of concentrated sunlight because concentrated sunlight has more irradiance power and contains more number of photons. These excess photons create more electron–hole pairs and hence more hydroxyl and superoxide radicals are formed to degrade MB dye faster.

4 Conclusions

The nanobelts of β-$AgVO_3$ have been prepared by simple hydrothermal method. The prepared thin nanobelts are of well crytalline and uniform having length between 5 and 10 μm with width 100–300 nm. These nanobelts have high capacity to absorb visible light and have optical band gap 1.96 eV. The β-$AgVO_3$ nanobelts exhibited high visible-light photocatalytic activity in the degradation of Methylene Blue dye under sunlight irradiation. The dye degradation rate becomes more than two times faster under concentrated sunlight irradiation. The concentrated sunlight has been utilized to degrade MB dye using solar concentrator coupled with optical fiber bundle. This new technology can be implemented to purify industrial wastewater using solar energy in a sustainable and cost-effective way.

Acknowledgements This work is financially supported by Sao Paulo Research Foundation (FAPESP), Brazil (Grant No. 2015/22828-6). Author J.S. Roy is grateful to FAPESP for providing postdoctoral research fellowship (Grant No. 2017/16826-6).

Compliance with ethical standards

Conflict of interest On behalf of all authors, the corresponding author states that there is no conflict of interest.

References

1. Laws EA (2017) Aquatic pollution: an introductory text. Wiley, Hoboken. ISBN 978-1-119-30450-0
2. Browne MA, Crump P, Niven SJ, Teuten E, Tonkin A, Galloway T, Thompson R (2011) Accumulation of microplastic on shorelines woldwide: sources and sinks. Environ Sci Technol 45:9175
3. Law KL, Morét-Ferguson S, Maximenko NA, Proskurowski G, Peacock EE, Hafner J, Reddy CM (2010) Plastic accumulation in the north atlantic subtropical gyre. Science 329:1185
4. Lapworth D, Baran N, Stuart M, Ward R (2012) Emerging organic contaminants in groundwater: a review of sources, fate and occurrence. Environ Pollut 163:287
5. Moss B (2008) Water pollution by agriculture. Phil Trans R Soc B 363:659
6. Kasprzyk-Hordern B, Dinsdale RM, Guwy AJ (2009) The removal of pharmaceuticals, personal care products, endocrine disruptors and illicit drugs during wastewater treatment and its impact on the quality of receiving waters. Water Res 43:363
7. Nelson ED, Do H, Lewis RS, Carr SA (2011) Diurnal variability of pharmaceutical, personal care product, estrogen and alkylphenol concentrations in effluent from a tertiary wastewater treatment facility. Environ Sci Technol 45:1228
8. Sirtori C, Zapata A, Oller I, Gernjak W, Agüera A, Malato S (2009) Decontamination industrial pharmaceutical wastewater by combining solar photo-Fenton and biological treatment. Water Res 43:661
9. Henao-Herreño LX, López-Tamayo AM, Ramos-Bonilla JP, Haas CN, Husserl J (2016) Risk of illness with salmonella due to consumption of raw unwashed vegetables irrigated with water from the bogotá river. Risk Anal 37:733
10. Singh KP, Mohan D, Sinha S, Dalwani R (2004) Impact assessment of treated/untreated wastewater toxicants discharged by sewage treatment plants on health, agricultural, and environmental quality in the wastewater disposal area. Chemosphere 55:227
11. Malathi A, Madhavan J, Ashokkumar M, Arunachalam P (2018) A review on $BiVO_4$ photocatalyst: activity enhancement methods for solar photocatalytic applications. Appl Catal A General 555:47
12. Linsebigler AL, Lu G, Yates JT (1995) Photocatalysis on TiO_2 surfaces: principles, mechanisms, and selected results. Chem Rev 95:735
13. Tang J, Durrant JR, Klug DR (2008) Mechanism of photocatalytic water splitting in TiO_2. Reaction of water with photoholes, importance of charge carrier dynamics, and evidence for four-hole chemistry. J Am Chem Soc 130:13885
14. Lan Y, Lu Y, Ren Z (2013) Mini review on photocatalysis of titanium dioxide nanoparticles and their solar applications. Nano Energy 2:1031
15. Choudhury B, Choudhury A (2013) Tailoring luminescence properties of TiO_2 nanoparticles by Mn doping. J Lumin 136:339
16. Molina J, Sanchez-Salas JL, Zuniga C, Mendoza E, Cuahtecontzi R, Garcia-Perez G, Gutierrez E, Bandala ER (2014) Low-temperature processing of thin films based on rutile TiO2 nanoparticles for UV photocatalysis and bacteria inactivation. J Mater Sci 49:786
17. Roy JS, Pal Majumder T, Dabrowski R (2015) Photoluminescence behavior of TiO_2 nanoparticles doped with liquid crystals. J Mol Struct 1098:351
18. Luo Y, Xu Y, Liu X, Xue H, Qian Q, Chen Q (2017) Design of Cu–Ce co-doped TiO_2 for improved photocatalysis. J Mater Sci 52:1265
19. Xiao Q, Si Z, Yu Z, Qiu G (2006) Sol–gel auto-combustion synthesis of samarium-doped TiO_2 nanoparticles and their photocatalytic activity under visible light irradiation. Mater Sci Eng B 137:189
20. Boningari T, Reddy Inturi SN, Suidan M, Smirniotis PG (2018) Novel one-step synthesis of nitrogen-doped TiO_2 by flame aerosol technique for visible-light photocatalysis: effect of synthesis parameters and secondary nitrogen (N) source. Chem Eng J 350:324
21. Choi W, Termin A, Hoffmann MR (1994) The role of metal ion dopants in quantum-sized TiO_2: correlation between photoreactivity and charge carrier recombination dynamics. J Phys Chem 98:13669
22. Umebayashi T, Yamaki T, Yamamoto S, Miyashita A, Tanaka S, Sumita T, Asai K (2003) Sulfur-doping of rutile-titanium dioxide by ion implantation: photocurrent spectroscopy and first-principles band calculation studies. J Appl Phys 93:5156

23. Lu Y, Shen Q, Yu Q, Zhang F, Li G, Zhang W (2016) Photoinduced in situ growth of Ag nanoparticles on $AgNbO_3$. J Phys Chem C 120:28712
24. Zhang Z, Wang W, Gao E (2014) Polypyrrole/$Bi2WO_6$ composite with high charge separation efficiency and enhanced photocatalytic activity. J Mater Sci 49:7325
25. Vu TA, Dao CD, Hoang TTT, Dang PT, Tran HTK, Nguyen KT, Le GH, Nguyen TV, Lee GD (2014) Synthesis of novel silver vanadates with high photocatalytic and antibacterial activities. Mater Lett 123:176
26. Choudhary S, Bisht A, Mohapatra S (2019) Facile synthesis, morphological, structural, photocatalytic and optical properties of $CoFe_2O_4$ nanostructures. SN Appl Sci 1:1613
27. Sharma G, Kumar A, Sharma S, Naushad M, Ahamad T, Al-Saeedi SI, Al-Senani GM, Al-kadhi NS, Stadler FJ (2018) Facile fabrication of $Zr_2Ni_1Cu_7$ trimetallic nano-alloy and its composite with Si_3N_4 for visible light assisted photodegradation of methylene blue. J Mol Liq 272:170
28. Wu SZ, Li K, Zhang WD (2015) On the heterostructured photocatalysts Ag_3VO_4/g-C_3N_4 with enhanced visible light photocatalytic activity. Appl Surf Sci 324:324
29. McNulty D, Ramasse Q, O'Dwyer C (2016) The structural conversion from α-$AgVO_3$ to β-$AgVO_3$: ag nanoparticle decorated nanowires with application as cathode materials for Li-ion batteries. Nanoscale 8:16266
30. Zhang X, Zhang J, Yu J, Zhang Y, Cui Z, Sun Y, Hou B (2018) Fabrication of $InVO_4$/$AgVO_3$ heterojunctions with enhanced photocatalytic antifouling efficiency under visible-light. Appl Catal B Environ 220:57
31. Wang K, Wu X, Zhang G, Li J, Li Y (2018) $Ba_5Ta_4O_{15}$ nanosheet/$AgVO_3$ nanoribbon heterojunctions with enhanced photocatalytic oxidation performance: hole dominated charge transfer path and plasmonic effect insight. ACS Sustain Chem Eng 6:6682
32. Zhang J, Ma Z (2018) Ag_3VO_4/AgI composites for photocatalytic degradation of dyes and tetracycline hydrochloride under visible light. Mater Lett 216:216
33. Liu B, Mu L, Han X, Zhang J, Shi H (2019) Highly efficient visible-light-driven photocatalytic activity of g-C_3N_4@Ag/$AgVO_3$ composites for dye degradation and bacterial inactivation. J Photochem Photobiol A Chem 380:111866
34. Gonzalez-Zavala F, Escobar-Alarcón L, Solís-Casados DA, Espinosa-Pesqueira M, Haro-Poniatowski E, Rodríguez-Castellón E, Rodríguez-Aguado E (2018) Synthesis and characterization of silver vanadates thin films for photocatalytic applications. Catal Today 305:102
35. Belver C, Adán C, García-Rodríguez S, Fernández-García M (2013) Photocatalytic behavior of silver vanadates: microemulsion synthesis and post-reaction characterization. Chem Eng J 224:24
36. Sharma G, Kumar A, Naushad M, Sharma S, Ghfar AA, Ahamad T, Si C, Stadler FJ (2019) Graphene oxide supported La/Co/Ni trimetallic nano-scale systems for photocatalytic remediation of 2-chlorophenol. J Mol Liq 294:111605
37. Bao S-J, Bao Q-L, Li C-M, Chen TP, Sun C-Q, Dong Z-L, Gan Y, Zhang J (2007) Synthesis and electrical transport of novel channel-structured beta-$AgVO_3$. Small 3:1174
38. Tian H, Wachs IE, Briand LE (2005) Comparison of UV and visible Raman spectroscopy of bulk metal molybdate and metal vanadate catalysts. J Phys Chem B 109:23491
39. Roy JS (2018) Comment to the article "Analysis of photoluminescence, UV absorbance, optical band gap and threshold voltage of TiO_2 nanoparticles dispersed in high birefringence nematic liquid crystal towards its application in display and photovoltaic devices" [J. Lumin. 192 (2017) 33–39]. J Lumin 203:41
40. Roy JS, Pal Majumder T, Schick C (2015) Optical characterization of CdS nanorods capped with starch. J Mol Struct 1088:95
41. Tauc J, Menth A (1972) States in the gap. J Non-Cryst Sol 8–10:569
42. Roy JS, Pal Majumder T, Dabrowski R, Mahato BK, Barman A (2015) Optical behaviour of CdS nanorods dispersed in liquid crystal. Adv Mater Lett 6:47
43. Jia P, Tan H, Liu K, Gao W (2018) Synthesis, characterization and photocatalytic property of novel ZnO/bone char composite. Mater Res Bul 102:45
44. Yang C, Dong W, Cui G, Zhao Y, Shi X, Xia X, Tang B, Wang W (2017) Highly efficient photocatalytic degradation of methylene blue by P2ABSA-modified TiO_2 nanocomposite due to the photosensitization synergetic effect of TiO_2 and P2ABSA. RSC Adv 7:23699